Atmospheric
Chemistry
and Physics

Supplement of

Comparison of six approaches to predicting droplet activation of surface active aerosol – Part 2: Strong surfactants

Sampo Vepsäläinen et al.

Correspondence to: Nønne L. Prisle (nonne.prisle@oulu.fi)

S1 Additional results

S1.1 Myristic acid and NaC$_{14}$ comparison

Figures S1 and S2 contain the Köhler curves and droplet surface tensions predicted with the simple partitioning, compressed film, and partial organic film models for myristic acid (continuous lines) and NaC$_{14}$ (dashed lines) for initial dry particle size of D_p = 50 nm at surfactant mass fractions ($w_\mathrm{p,sft}$) of 0.2, 0.5, 0.8 and 0.95 in the dry particles. Calculations with the other surface activity models are not performed due to the lack of required input data for water–myristic acid–NaCl mixture. Table S1 contains the droplet diameters, supersaturations, and surface tensions at the critical point of cloud droplet activation corresponding to Figs. S1 and S2. The minimum surface thickness (δ_sft) with the partial organic film calculations was set to a constant value of 0.5 nm. The same compressed film model parameters (A_0, m_σ, C_0) were used for both compounds during the calculations of the compressed film model.

Figure S1 shows that the differences in the predictions between myristic acid and NaC$_{14}$ are consistent, preserving the shape of the Köhler curves with the different models. The SS$_\mathrm{c}$ for droplets containing myristic acid are higher and the d_c are smaller than for NaC$_{14}$ predictions (Tables S1, S2 and S3). The predictions of the compressed film model show a maximum 15 % relative increase in SS$_\mathrm{c}$ and a maximum 13 % decrease in d_c for $w_\mathrm{p,sft} = 0.8$ when the particles contain myristic acid instead of NaC$_{14}$ (Table S3). The predictions of the simple partitioning model show a maximum 15 % increase in SS$_\mathrm{c}$ and a 12 % decrease in d_c for the same conditions. The maximum difference between myristic acid and NaC$_{14}$ for the predictions of the partial organic model is greater, the d_c of the acid is smaller by a maximum of 65 %, and the supersaturation is greater than with NaC$_{14}$ by a maximum of 32 %, both at $w_\mathrm{p,sft} = 0.95$. This large change in d_c is a result of the critical point moving to a droplet size where the organic surface film has not yet broken (Fig. S1(d)). This is a consequence of the higher surface tension of pure myristic acid than the surface tension at the CMC for binary water-NaC$_{14}$.

Figure S2 shows the droplet surface tensions along the Köhler curves predicted with the three models. The simple partitioning model always assumes a surface tension equal to that of water. The predictions of the compressed film model are similar for both compounds with a shift in droplet sizes. The surface tension predicted with the partial organic film model shifts, and the lower limit of the surface tension is different, but the overall shape of the surface tension curves remains similar for both surfactants. The droplet surface tension at activation is similar for both cases in Figs. S2(a) –S2(c) (Tables S2 and S3). In Fig. S2(d), the change in d_c between the acid and NaC$_{14}$ also leads to considerably lower σ_c of the partial film model for the droplets containing myristic acid.

S1.2 Compressed film model sensitivity to surfactant molar volume

Figures S3 and S4 show the predictions of Köhler curves and the droplet surface tension during droplet growth with the compressed film model for particles containing myristic acid with variable molar volume compared to predictions for particles containing NaC$_{14}$, both mixed with NaCl. The analysis is provided because the molar volumes of the acid and its sodium salt are different but the same model specific parameters (Sect. 2.2.3 of the main paper) have been used for both myristic acid and NaC$_{14}$ due to lack of suitable data to fit parameters specifically for NaC$_{14}$. A more detailed analysis of the compressed model sensitivity is available in the Supplement of Vepsäläinen et al. (2022).

Fig. S3 shows that varying the myristic acid molar volume only significantly affects the visible Köhler curves at higher $w_\mathrm{p,sft}$ (Figs. S3(c) and (d)) and is more focused on smaller droplet sizes. The critical point is only significantly affected in Fig. S3(d), where the predicted critical point of the droplets containing NaC$_{14}$ is in the shaded red area, which denotes the different levels of variation in the myristic acid molar volume. The predicted intersection corresponds to a rough decrease of ~ 30 % in the molar volume of myristic acid. Calculated with the molar masses and solid phase densities given in Table 1 of the main article, the myristic acid molar volume is about 27 % larger than that of NaC$_{14}$, which is in good agreement with Fig. S3(d).

Figure S4 shows how the predicted surface tension curve remains the same shape with varying molar volume. The droplet size where the surface tension of water is reached and the rising part of the curve leading to it are shifted with varying molar volume.

Table S1. The critical droplet diameters (d_c), supersaturations (SS$_c$) and surface tensions (σ_c) predicted with the different models for particles comprising myristic acid or NaC$_{14}$ mixed with NaCl at 298.15 K for D_p = 50 nm. The partial organic film calculations were performed at a constant minimum surface thickness δ_{sft} = 0.5 nm.

Parameter	d_c (nm)	SS$_c$ (%)	σ_c (mN m^{-1})	d_c (nm)	SS$_c$ (%)	σ_c (mN m^{-1})	d_c (nm)	SS$_c$ (%)	σ_c (mN m^{-1})
					Myristic acid				
$w_{p,sft}$		Simple			Compressed film			Partial organic film	
0.2	372	0.38	72.0	384	0.37	72.0	404	0.35	68.2
0.5	254	0.55	72.0	262	0.54	72.0	335	0.42	61.7
0.8	148	0.97	72.0	152	0.94	72.0	287	0.49	54.0
0.95	85	1.83	72.0	116	1.58	71.9	112	0.59	32.1
					NaC$_{14}$				
$w_{p,sft}$		Simple			Compressed film			Partial organic film	
0.2	392	0.36	72.0	406	0.34	72.0	428	0.33	68.2
0.5	284	0.5	72.0	293	0.48	72.0	376	0.37	61.6
0.8	169	0.84	72.0	174	0.81	72.0	334	0.42	53.9
0.95	94	1.62	72.0	131	1.39	72.0	315	0.44	49.5

Table S2. The absolute differences (Δ = myristic acid - NaC$_{14}$ predictions) in critical droplet diameters (d_c), supersaturations (SS$_c$) and surface tensions (σ_c) between myristic acid and NaC$_{14}$ corresponding to Table S1. The absolute difference were calculated with the exact d_c, SS$_c$, and σ_c values and rounded to the displayed degree.

Parameter	Δd_c (nm)	ΔSS$_c$ (%)	$\Delta\sigma_c$ (mN m^{-1})	Δd_c (nm)	ΔSS$_c$ (%)	$\Delta\sigma_c$ (mN m^{-1})	Δd_c (nm)	ΔSS$_c$ (%)	$\Delta\sigma_c$ (mN m^{-1})
$w_{p,sft}$		Simple			Compressed film			Partial organic film	
0.2	-21	0.02	0	-23	0.02	0	-24	0.02	0.1
0.5	-29	0.06	0	-31	0.06	0	-41	0.05	0.1
0.8	-21	0.13	0	-22	0.12	0	-47	0.07	0.1
0.95	-9	0.21	0	-15	0.19	-0.1	-204	0.14	-17.4

S1.3   Partial organic film model constant δ_{sft}

Figure S5 shows the supersaturation predicted with the monolayer and partial organic film models for D_p = 50 nm at $w_{p,sft}$ = 0.2, 0.5, 0.8 and 0.95. The partial film model calculations were performed at the minimum surface layer thickness (δ_{sft}) equal to that calculated by the monolayer model (δ_{ML}) and with a constant δ_{sft} = 0.5 nm ($\delta_{0.5}$). The δ_{sft} values calculated with the monolayer model for NaC$_{14}$ are between 0.39 and 0.90 nm, depending on the droplet size (smaller droplets have a larger surface thickness).

Figure S5 shows that the main effect of the different δ_{sft} is a minor one for the critical point. The SS$_c$ is slightly higher with constant δ_{sft} for all $w_{p,sft}$, while d_c is slightly smaller in Figs. S5(a) and (b) and larger in Figs. S5(c) and (d).

Figure S6 contains the droplet surface tensions corresponding to the Köhler curves in Fig. S5. The main difference between the two partial organic film model predictions is at smaller droplet sizes, where the constant surface thickness leads to the organic surface film breaking at larger droplet sizes. Furthermore, the overall shape of the predicted surface tension curve is slightly different with the constant surface thickness, but only to a small degree. The constant δ_{sft} leads to increased σ_c and the difference increases with $w_{p,sft}$.

Table S3. The ratios of critical droplet diameters (d_c), supersaturations (SS_c) and surface tensions (σ_c) for the predictions of the different models between myristic acid and NaC_{14} corresponding to Table S1. The ratios were calculated with the exact d_c, SS_c, and σ_c values and rounded to the displayed degree.

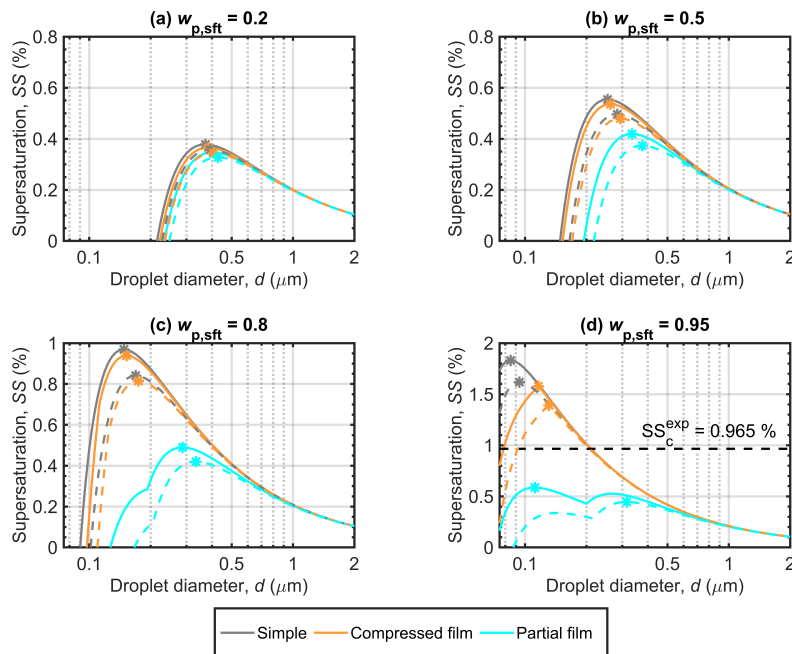| Parameter	$\frac{d_c^{acid}}{d_c^{NaC_{14}}}$	$\frac{SS_c^{acid}}{SS_c^{NaC_{14}}}$	$\frac{\sigma_c^{acid}}{\sigma_c^{NaC_{14}}}$	$\frac{d_c^{acid}}{d_c^{NaC_{14}}}$	$\frac{SS_c^{acid}}{SS_c^{NaC_{14}}}$	$\frac{\sigma_c^{acid}}{\sigma_c^{NaC_{14}}}$	$\frac{d_c^{acid}}{d_c^{NaC_{14}}}$	$\frac{SS_c^{acid}}{SS_c^{NaC_{14}}}$	$\frac{\sigma_c^{acid}}{\sigma_c^{NaC_{14}}}$
$w_{p,sft}$	Simple			Compressed film			Partial organic film		
0.2	0.95	1.06	1.0	0.94	1.06	1.0	0.94	1.06	1.0
0.5	0.9	1.12	1.0	0.89	1.12	1.0	0.89	1.12	1.0
0.8	0.88	1.15	1.0	0.87	1.15	1.0	0.86	1.17	1.0
0.95	0.91	1.13	1.0	0.89	1.13	1.0	0.35	1.32	0.65

Figure S1. The Köhler curves predicted with the simple partitioning, compressed film, and partial organic film models at different surfactant mass fractions ($w_{p,sft}$) in particles at $D_p = 50$ nm containing myristic acid (continuous lines) and NaC_{14} (dashed lines), both mixed with NaCl. The critical points are also marked. Note that the vertical axis scaling changes between the panels.

Table S4 contains the critical droplet properties as well as the absolute differences and the ratios between the predicted critical droplet properties for the partial organic film model calculations performed with a δ_{sft} equal to that of the monolayer model or with 0.5 nm. The calculation of the difference was performed as $\delta_{ML} - \delta_{0.5}$ with the predicted critical properties, and then rounded to the accuracy in Table S4.

S1.4 Extended dry particle size range

Figures S7 and S8 contain predictions of critical supersaturation and diameter for particles of NaC_{14} mixed with NaCl for $D_p = 50 - 200$ nm. The inter-model variation between the different partitioning models remains largely the same for particles
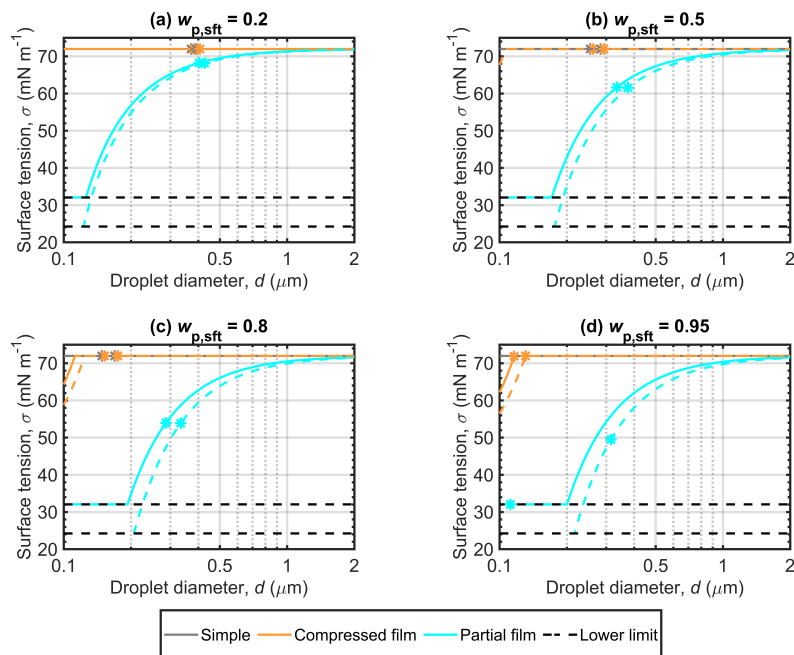
3

Figure S2. Droplet surface tensions along the Köhler curves predicted with the simple partitioning, compressed film and partial organic film models at different surfactant mass fractions ($w_{p,sft}$) in the particles ($D_p = 50$ nm) for myristic acid (continuous lines) and NaC_{14} (dashed lines) mixed with NaCl. The critical points are also marked. The lower limit for the surface tension (marked in the legend as "Lower limit") for droplets containing NaC_{14} is the surface tension of the binary NaC_{14}-water mixture at the CMC, while for myristic acid, the lower limit is that of the pure acid surface tension (Zhang et al., 2018; Di Nicola et al., 2016).

of all sizes with a given mass fraction of NaC_{14}. There is variation with the Gibbs model due to the effects related to the CMC
65 discussed in more detail in the main article.

S2 Calculation details

The Supplement of Vepsäläinen et al. (2022) contains more general information on various calculations not detailed here.

S2.1 Water activity

The water activity calculated as the corrected mole fraction:

$$70 \quad a_w = \frac{n_w}{n_w + i_{sft} n_{sft} + i_{salt} n_{salt}}, \tag{S1}$$

where n_w, n_{sft}, and n_{salt} are the amounts of water, surfactant, and inorganic salt, while i_{sft} and i_{salt} are the dissociation factors for for the surfactant and the inorganic salt. For both NaCl and NaC_{14}, a dissociation factor of two was used. A dissociation factor of one was used for myristic acid.

The AIOMFAC-based (AIOMFAC-web, 2023) water activity fit used for the simple partitioning model (Prisle et al., 2011)
75 and the partial organic film model (Ovadnevaite et al., 2017) for binary solutions of water-NaCl at 298.15 K is

$$a_w = (55.9521 \cdot x_{salt}^2 + 11.9208 \cdot x_{salt} + 1.2668) \cdot \exp(-11.7538 \cdot x_{salt}) - 0.2668 \cdot \exp(-4.1305 \cdot x_{salt}), \tag{S2}$$

where x_{salt} is the mole fraction of the inorganic salt.
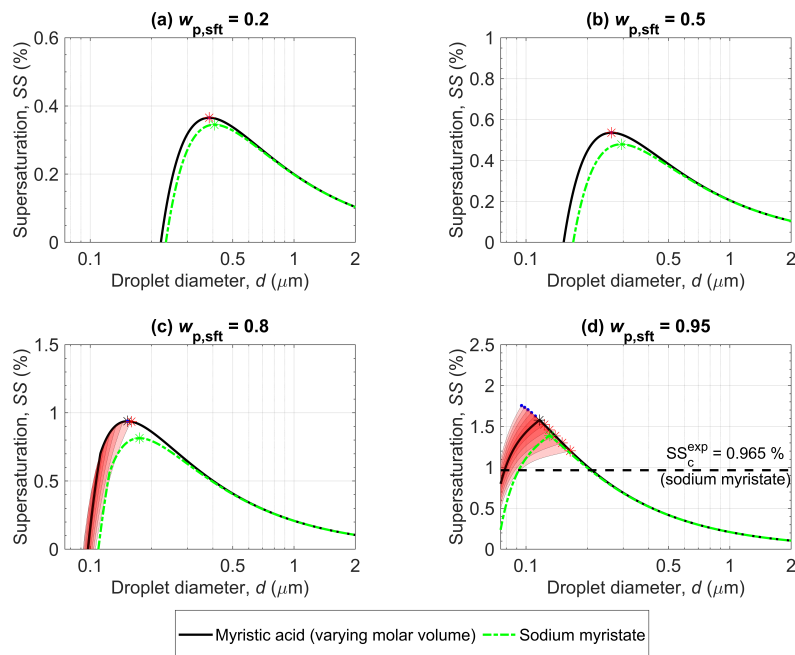
Figure S3. Supersaturation predicted for $D_p = 50$ nm with the compressed film model at different surfactant mass fractions ($w_{p,sft}$) for myristic acid (black line) with varying molar volume visible as shaded red areas corresponding to $\Delta\% = \pm10\%, \pm20\%, \pm30, \pm40\%$ and $\pm50\%$ variations. The variation is calculated as $\bar{v} \cdot X$ where X is the multiplier taken as $(100\% \pm \Delta\%)/100$. The critical points predicted with positive changes in the molar volume are marked in blue dots. The critical points predicted with negative changes are marked in red asterisks. The predictions for NaC_{14}–NaCl droplets (green dashed line) are visible, as is SS_c^{exp} from Prisle et al. (2008) in panel (d). Note that the vertical axis scaling changes between the panels.

S2.2 Surface tension

The surface tension of pure NaC_{14} is extended from the aqueous binary fit, and therefore is the surface tension at the CMC. Surface tension of pure NaCl is calculated according to the equation given by Vanhanen et al. (2008). The binary surface tension of water-NaCl is calculated according to Vanhanen et al. (2008). The binary surface tension of binary water–NaC_{14} was determined from Wen et al. (2000) though data digitized by using the *WebPlotDigitizer* (Rohatgi, 2021). The fit was made at 298.15 K and follows the form of the Szyszkowski–Langmuir equation (Szyszkowski, 1908) given in Prisle et al. (2008). The fit equation (in N m^{-1}) is

$$\sigma = \sigma_w - 0.007042\ln(1 + 2.81 \cdot 10^7 \cdot \min(x, x_{CMC})), \tag{S3}$$

where σ_w is the surface tension of water (IAPWS, 2014), x is the mole fraction of NaC_{14} and x_{CMC} is the critical micelle concentration as a mole fraction.

The ternary surface tension of water, NaC_{14} and NaCl was also fitted to the digitized (Rohatgi, 2021) data of Wen et al. (2000) using the form of the Szyszkowski–Langmuir equation given by Prisle et al. (2010):

$$\sigma = \sigma_w + \left(\frac{d\sigma_{NaCl}}{dm_{NaCl}}\right)m_{NaCl} - a\ln(1 + m_{sft}/b) \tag{S4}$$
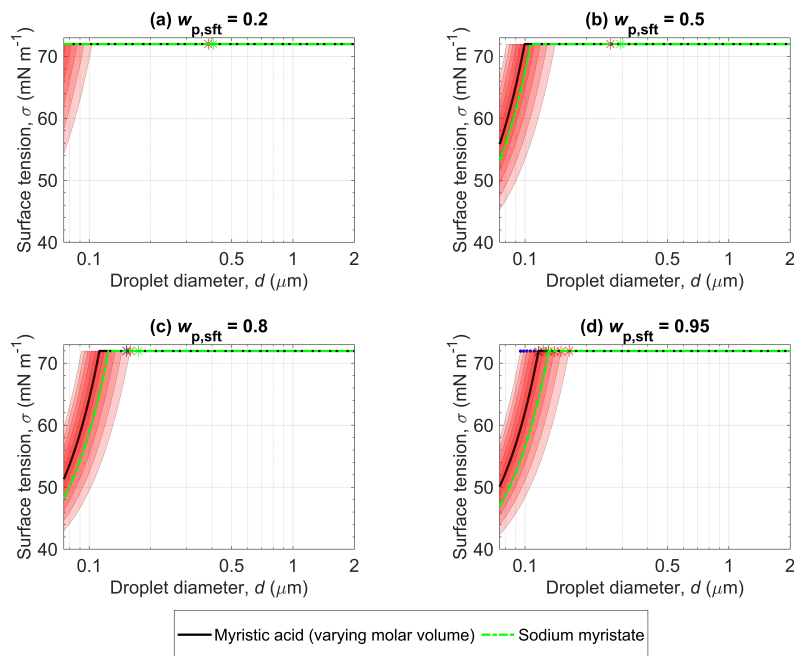
Figure S4. Droplet surface tensions corresponding to Fig. S3 predicted with the compressed film model at different $w_{\mathrm{p,sft}}$ for myristic acid–NaCl $D_{\mathrm{p}} = 50$ nm particles (black line) with varying molar volume (red shaded areas corresponding to $\Delta\% = \pm10\%, \pm20\%, \pm30, \pm40\%$ and $\pm50\%$ variations). The variation is calculated as $\bar{v} \cdot X$ where X is the multiplier taken as $(100\% \pm \Delta\%)/100$. The critical points predicted with positive changes in the molar volume are marked in blue dots, and the critical points predicted with negative changes are marked in red asterisks. The droplet surface tensions predicted for NaC_{14}–NaCl droplets (green dashed line) are also included.

where m is the molality of NaCl or surfactant depending on the index, and

$$a = a_1 + a_2 w_{\mathrm{sft}} + a_3 w_{\mathrm{sft}}^2, \tag{S5}$$

$$b = b_1 + b_2 w_{\mathrm{sft}} + b_3 w_{\mathrm{sft}}^2, \tag{S6}$$

$$w_{\mathrm{sft}} = \frac{x_{\mathrm{sft}} M_{\mathrm{sft}}}{x_{\mathrm{sft}} M_{\mathrm{sft}} + x_{\mathrm{NaCl}} M_{\mathrm{NaCl}}}. \tag{S7}$$

95 The mole fractions x_{sft} and x_{NaCl} above are the mole fractions in the ternary aqueous mixture. The parameters for Eqs. (S5) and (S6) can be found in Table S5. Eq. (S4) gives the surface tension in units of $\mathrm{mN\ m^{-1}}$ with the given parameters and therefore σ_{w} needs to be in the same units. The salt gradient (Vanhanen et al., 2008; Prisle et al., 2010) in Eq. (S4) is

$$\frac{d\sigma_{\mathrm{NaCl}}}{dm_{\mathrm{NaCl}}} = 1.61\ (\mathrm{mN\ m^{-1}})/(\mathrm{mol\ kg^{-1}}).$$

The surface tension of the ternary solution cannot be lower than the pure surfactant or, in this case, the surface tension at the
100 CMC for the binary solution of water and NaC_{14}.

Pure surface tension of myristic acid is calculated using the method of Zhang et al. (2018) with initial data from Di Nicola et al. (2016).

Table S4. The critical droplet diameters (d_c), supersaturations (SS_c) and surface tensions (σ_c) for partial organic film model simulations with surface thickness equal to the output of the monolayer model (δ_{ML} and a constant $\delta_{sft} = 0.5$ nm, denoted as $\delta_{0.5}$). The absolute differences and ratios between the predicted critical properties are also displayed. The absolute differences and ratios were calculated with the exact d_c, SS_c, and σ_c values and rounded to the displayed degree.

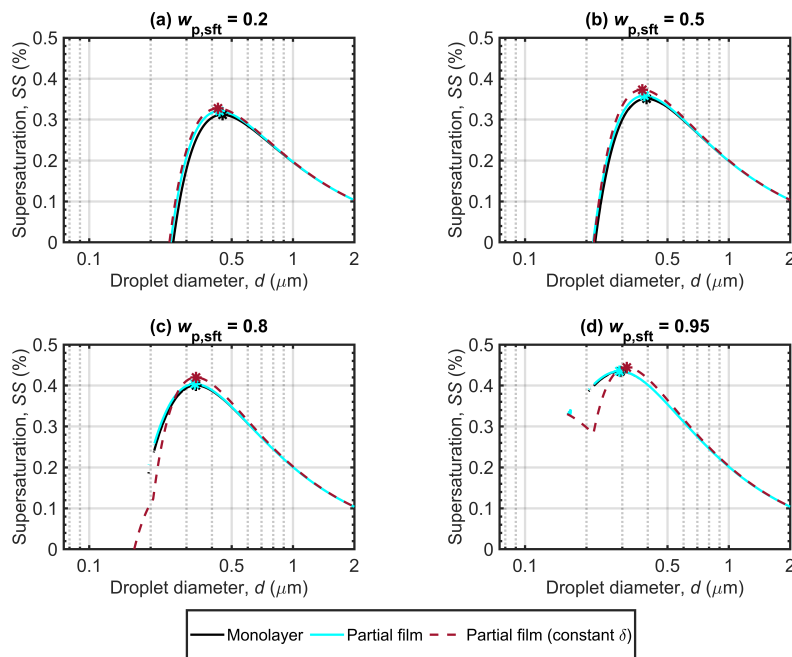| Parameter	d_c (nm)	SS_c (%)	σ_c (mN m^{-1})	d_c (nm)	SS_c (%)	σ_c (mN m^{-1})
$w_{p,sft}$		Partial organic film (δ_{ML})			Partial organic film ($\delta_{0.5}$)	
0.2	435	0.32	67.3	428	0.33	68.2
0.5	385	0.36	60.2	376	0.37	61.6
0.8	330	0.4	51.6	334	0.42	53.9
0.95	290	0.44	45.1	316	0.44	49.5
		$\delta_{ML} - \delta_{0.5}$			$\delta_{ML}/\delta_{0.5}$	
$w_{p,sft}$	Δd_c (nm)	ΔSS_c (%)	$\Delta\sigma_c$ (mNm^{-1})	$\dfrac{d_{c,ML}}{d_{c,0.5}}$	$\dfrac{SS_{c,ML}}{SS_{c,0.5}}$	$\dfrac{\sigma_{c,ML}}{\sigma_{c,0.5}}$
0.2	7	-0.01	-0.8	1.02	0.98	0.99
0.5	9	-0.01	-1.4	1.02	0.96	0.98
0.8	-5	-0.02	-2.3	0.99	0.96	0.96
0.95	-25	-0.01	-4.4	0.92	0.98	0.91

Figure S5. The Köhler curves for initial particles of NaC$_{14}$ mixed with NaCl predicted with the monolayer and partial organic film models for $D_p = 50$ nm at different surfactant mass fractions ($w_{p,sft}$) of 0.2, 0.5, 0.8, and 0.95. The critical points are also marked.

S2.3 Density

The density of pure liquid NaC$_{14}$ is extended from the density of binary solution of water and NaC$_{14}$. The binary aqueous
105 density is estimated using the method of Calderón and Prisle (2021), as is the ternary density of water, NaC$_{14}$ and NaCl.
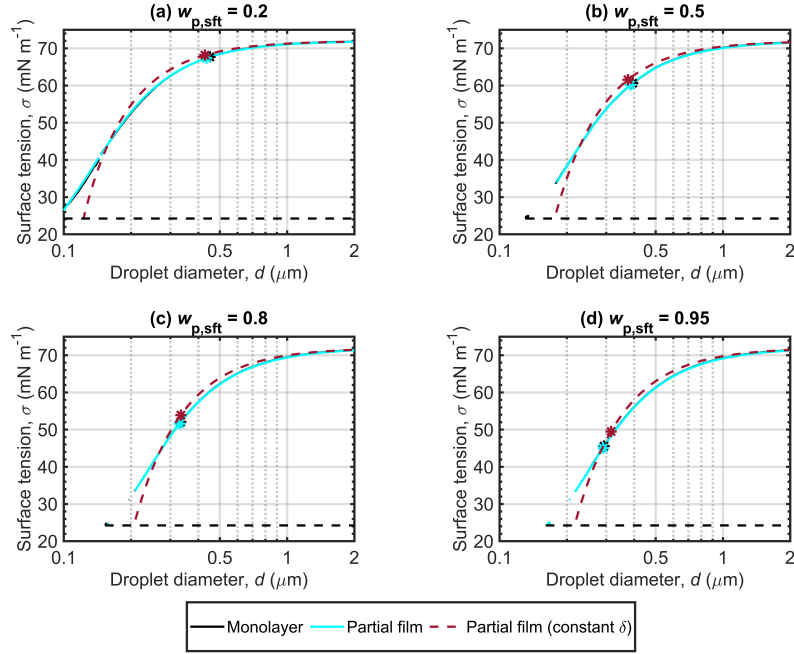
Figure S6. The droplet surface tensions along the Köhler curves for initial particles of NaC_{14} mixed with NaCl predicted with the monolayer and partial organic film models for $D_p = 50$ nm at different surfactant mass fractions ($w_{p,sft}$) of 0.2, 0.5, 0.8, and 0.95. The critical points are also marked, as well as the lower surface tension limit of the droplet (the surface tension at the CMC).

Table S5. Fitting parameters for Eqs. (S5) and (S6).

i	1	2	3
a_i	15.4246	-2.9546	-4.5712
b_i	$0.0776 \cdot 10^{-4}$	$0.3776 \cdot 10^{-4}$	$-0.4262 \cdot 10^{-4}$

According to the method, the density of binary aqueous surfactant solutions is calculated using the apparent molal volume of the surfactant Φ_{sft} as

$$\rho = \frac{1 + m_{sft} M_{sft}}{1/\rho_w + 1 \cdot 10^{-6} \Phi_{sft} m_{sft}} \tag{S8}$$

110 where m_{sft} and M_{sft} are the molality and the molar mass of the surfactant, respectively, and ρ_w is the density of pure water (Pátek et al., 2009). The apparent partial molal volume of the surfactant changes due to micellization and its value can be calculated as

$$\Phi_{sft} = H\left(CMC - m_{sft}\right)\left(\Phi_{sft}^{\infty} + A_v\sqrt{m_{sft}} + B_{sft}^V m_{sft}\right) + H\left(m_{sft} - CMC\right)\left((1-\xi)\Phi_{sft}^{CMC} + \xi V_{mic}\right), \tag{S9}$$

where CMC is in molal units, Φ_{sft}^{∞} and Φ_{sft}^{CMC} are the apparent molal volume of the surfactant at infinite dilution and at the CMC in $cm^3\,mol^{-1}$, respectively, and H is the Heaviside step function. In addition, the fraction of micellization ξ is estimated 115 from a concentration-dependent parametrization of the CMC as (Lisi et al., 1980)

$$\xi = \left(\frac{\left(sgn\left(m_{sft} - CMC\right) + 1\right)}{2}\right)\frac{m_{sft} - CMC}{m_{sft}}. \tag{S10}$$
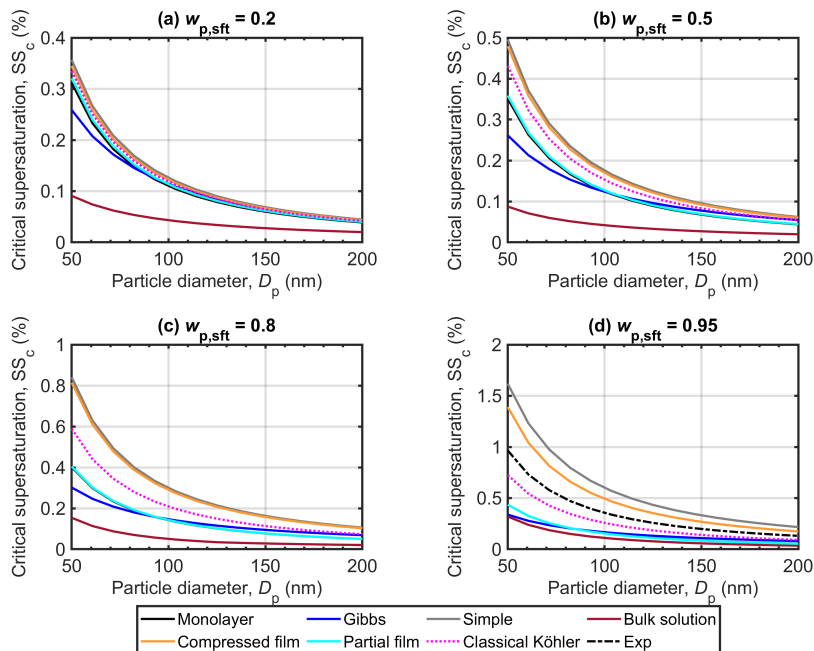
Figure S7. The critical supersaturation predicted for dry particles of NaC_{14} mixed with NaCl for D_p = 50 – 200 nm with the different models. The line labeled as "Exp" corresponds to Eq. (S26) (Prisle et al., 2008) for particles of pure NaC_{14}.

The model parameter B_{sft}^V is used to include the effect of surfactant-surfactant interactions with consistent units of cm^3 mol^{-2} kg. These model parameters have been obtained from Vikingstad et al. (1978) and Blanco et al. (2005) for NaC_{14} or a similar compound if direct data was not available.

The partial molar volumes at 25°C are from Vikingstad et al. (1978). At infinite dilution $\Phi_{sft}^{\infty} = 226.4$ cm^3 mol^{-1} and at the CMC $\Phi_{sft}^{CMC} = 226.5$ cm^3 mol^{-1}.

In the absence of data for NaC_{14}, a B_{sft}^V parametrization for sodium dodecanoate was used based on Blanco et al. (2005) as

$$B_{sft}^V = -35.26 \exp\left(-\left(\frac{(T-317.3)}{7.893}\right)^2\right) + 90.18 \exp\left(-\left(\frac{(T-301.6)}{47.41}\right)^2\right). \tag{S11}$$

The variable V_{Mic} is the surfactant molal volume in micellar form. Its value depends on the change in molar volume experienced by the surfactant during micellization as

$$V_{mic} = \Phi_{sft}^{CMC} + \Delta V_{mic}. \tag{S12}$$

The ΔV_{mic} is a temperature-dependent parameter that here we have taken at 25°C from Vikingstad et al. (1978): $\Delta V_{mic} = 14.3$ cm^{3}mol^{-1}.

The variable A_v represents the Debye-Hückel limiting slope in volume units, $\left(\text{cm}^3 \text{ kg}^{1/2} \text{ mol}^{-3/2}\right)$ calculated as

$$\begin{aligned} A_v = 1.50619 + 0.0130073(T-273.15) + 4.8307 \times 10^{-5}(T-273.15)^2 + 8.95087 \times 10^{-7}(T-273.15)^3 \\ -3.727 \times 10^{-9}(T-273.15)^4 + 2.3942 \times 10^{-11}(T-273.15)^5 \end{aligned} \tag{S13}$$

according to Millero (2014). Eqs. (S8)-(S13) are used to estimate the density of aqueous NaC_{14}.
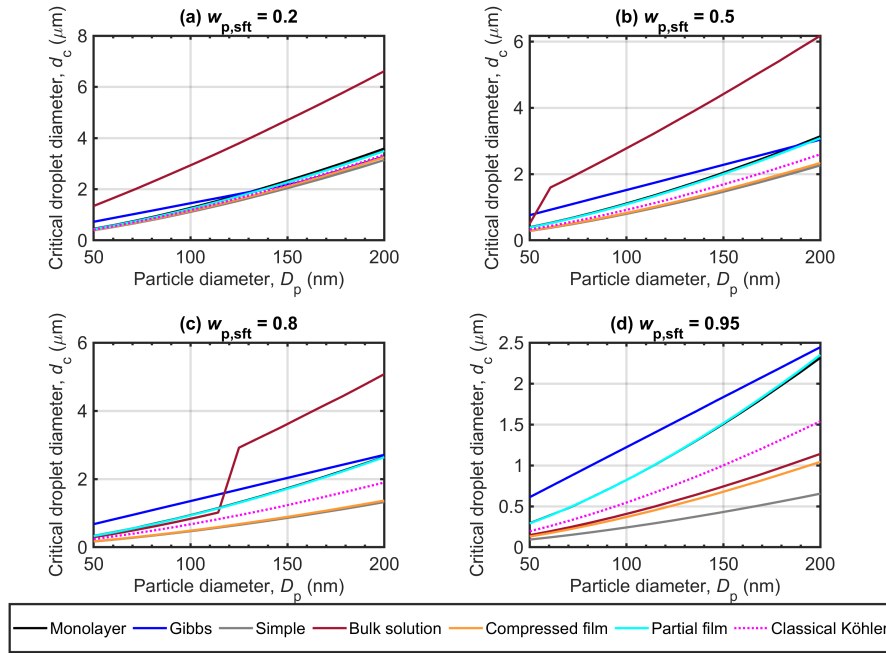
Figure S8. The critical droplet diameters predicted for dry particles of NaC_{14} mixed with NaCl for $D_p = 50 - 200$ nm with the different models.

The ternary density of the solution of water, NaC_{14} and NaCl is estimated using a pseudo- binary approach that uses the mean apparent molal volume ($\bar{\Phi}$) of the solutes from the mixing rule of Young and Smith (1954)

$$\bar{\Phi} = \frac{m_{sft}\Phi_{sft} + m_{NaCl}\Phi_{NaCl}}{m_{sft} + m_{NaCl}}. \tag{S14}$$

135 The density of the ternary solution is calculated as

$$\rho = \frac{1 + m_{sft}M_{sft} + m_{NaCl}M_{NaCl}}{1/\rho_w + (m_{sft} + m_{NaCl})\bar{\Phi} \cdot 10^{-6}}. \tag{S15}$$

The apparent molal volume of the surfactant is calculated with equation (S9). However, now the presence of salt affects micellization and therefore the parameters of Eq. (S9). The fraction of counterions associated with micelles in aqueous solutions was not available for NaC_{14}, and therefore a value reported by Vikingstad et al. (1978) for aqueous sodium dodecanoate was

140 used $\beta_0 = 0.74$. The effect of NaCl (ternary solution) according to Calderón and Prisle (2021) can be accounted for with

$$\beta = \beta_0 + 2.2297m_{NaCl}. \tag{S16}$$

For the ternary solution, the effect of the inorganic salt on the volume change during micellization ΔV_{mic}^{ter} is defined via equation

$$\Delta V_{mic}^{ter} = (\Delta V_{mic} - 4.681\beta_0) - 23.35m_{NaCl} + 4.681\beta \tag{S17}$$

and then if $\Delta V_{mic}^{ter} > 0$

145 $$V_{mic} = \Phi_{sft}^{CMC} + \Delta V_{mic}^{ter}. \tag{S18}$$

Otherwise, Eq. (S12) is used. The apparent partial molal volume of the salt is calculated according to the model of Rogers and Pitzer (1982) as

$$\Phi_{\mathrm{NaCl}} = \Phi_{\mathrm{NaCl}}^{\infty} + 2A_v \frac{\ln(1 + b\sqrt{I})}{2b} + 2RT \left(m_{\mathrm{NaCl}} B_{\mathrm{NaCl}}^V + m_{\mathrm{NaCl}}^2 C_{\mathrm{NaCl}}^V \right), \tag{S19}$$

where Φ_{NaCl} and $\Phi_{\mathrm{NaCl}}^{\infty}$ are the apparent partial molal volume of NaCl in the solution and at a hypothetical infinite dilute solution, I is the ionic strength of the solution defined as $I = 0.5 \sum z_i^2 m_i$, where z_i is the ion valence; b is a model parameter equal to $1.2\ \mathrm{kg}^{0.5}\ \mathrm{mol}^{-0.5}$ for all electrolyte systems. The value of A_v is calculated via equation (S13).

Calderón and Prisle (2021) presents the following equations for calculating the parameters $\Phi_{\mathrm{NaCl}}^{\infty}$, B_{NaCl}^v and C_{NaCl}^v:

$$\Phi_{\mathrm{NaCl}}^{\infty} = -0.001462T^2 + 0.9609T - 139.9, \tag{S20}$$
$$B_{\mathrm{NaCl}}^v = 0.2694\exp(-0.03379T) + 2.611 \times 10^{-8}\exp(0.01245 \cdot T) \text{ and} \tag{S21}$$
$$C_{\mathrm{NaCl}}^v = -0.04196\exp(-0.03719T). \tag{S22}$$

Eqs.(S20)–(S22) have been acquired by fitting temperature-dependent models of each parameter to the experimental densities of NaCl solutions ($T = 273 - 373$ K and p= 1 bar) presented by Pitzer et al. (1984). Both the binary and ternary densities of the water–surfactant or water–surfactant–salt solutions are constrained by the pure compound densities.

Pure density of liquid myristic acid is calculated from Noureddini et al. (1992)

$$\rho = (-6.727 \cdot 10^{-4} \cdot (T - 273.15) + 8.9909 \cdot 10^{-1}) \cdot 1000. \tag{S23}$$

Pure density of liquid NaCl is calculated using an extrapolation (in the temperature range) of Janz (1980). The binary density of water and NaCl is estimated as explained in Calderón and Prisle (2021)

$$\rho = \left(\frac{m_{\mathrm{NaCl}} \cdot \Phi_{\mathrm{NaCl}} + 1000 \cdot V_1^{\circ}/M_{\mathrm{w}})}{1000 + m_{\mathrm{NaCl}} M_{\mathrm{NaCl}}} \right)^{-1} \cdot 1000, \tag{S24}$$

where

$$V_1^{\circ} = 42.8\exp(-0.01254T) + 12.6\exp(0.001014T) \tag{S25}$$

is a temperature-dependent relationship fitted to experimental data for this variable, and the molar masses are in $\mathrm{g\ mol}^{-1}$. The molal volume of salt Φ_{NaCl} is calculated with Eq. (S19).

S2.4 Critical micelle concentration

The calculations of the present work employ the critical micelle concentration of a binary mixture of water and NaC_{14}. The CMC was determined from the digitized (Rohatgi, 2021) data from Wen et al. (2000). The same data set used for the ternary surface tension fit. This was done to ensure internal consistency of the simulations and to avoid any unrealistic values or sudden step-increases or decreases in the surface tension fits.

The CMC was determined directly as a mole fraction of the surfactant from a $(\ln(x_{\mathrm{sft}}), \sigma)$ plot via fitting of two straight lines, one to the linearly decreasing surface tension and one to the baseline of minimal surface tension. The intersection point of the two lines is taken as the CMC. Determined in this way, $x_{\mathrm{CMC}} = 3.1191 \cdot 10^{-5}$ with the corresponding surface tension $\sigma_{\mathrm{CMC}} = 24.2483\ \mathrm{mNm}^{-1}$.

S2.5 NaC_{14} SS_c^{exp}

Prisle et al. (2008) measured experimental critical supersaturations as a function of dry particle diameter, and fitted the results as power functions. The equation given by Prisle et al. (2008) for NaC_{14} is

$$y = 271.74 \cdot x^{-1.4417}, \tag{S26}$$

where y denotes the SS_c and x the dry particle diameter.

References

AIOMFAC-web: version 3.04, https://aiomfac.lab.mcgill.ca, accessed: 2023-04-13, 2023.

Blanco, E., González-Pérez, A., Ruso, Juan, M., Pedrido, R., Prieto, G., and Sarmiento, F.: A comparative study of the physicochemical properties of perfluorinated and hydrogenated amphiphiles, J. Colloid Interface Sci., 288, 247–260, https://doi.org/https://doi.org/10.1016/j.jcis.2005.02.085, 2005.

Calderón, S. M. and Prisle, N. L.: Composition dependent density of ternary aqueous solutions of ionic surfactants and salts, J. Atmos. Chem, 78, 99–123, https://doi.org/10.1007/s10874-020-09411-8, 2021.

Di Nicola, G., Coccia, G., and Pierantozzi, M.: A new equation for the surface tension of carboxylic acids, Fluid Phase Equilib., 417, 229 – 236, https://doi.org/https://doi.org/10.1016/j.fluid.2016.03.001, 2016.

International Association for the Properties of Water and Steam (IAPWS): Revised Release on Surface Tension of Ordinary Water Substance: IAPWS R1-76 (2014), Moscow, http://www.iapws.org/relguide/Surf-H2O.html, last access: 18.3.2020, 2014.

Janz, G. J.: Molten Salts Data as Reference Standards for Density, Surface Tension, Viscosity, and Electrical Conductance: KNO3 and NaCl, J. Phys. Chem. Ref. Data, 9, 791–830, https://doi.org/10.1063/1.555634, 1980.

Lisi, R. D., Perron, G., and Desnoyers, J. E.: Volumetric and thermochemical properties of ionic surfactants: sodium decanoate and octylamine hydrobromide in water, Can. J. Chem., 58, 959–969, https://doi.org/10.1139/v80-152, 1980.

Millero, F.: Estimation of the Partial Molar Volumes of Ions in Mixed Electrolyte Solutions Using the Pitzer Equations, J. Solution Chem., 43, 1448–1465, https://doi.org/10.1007/s10953-014-0213-0, 2014.

Noureddini, H., Teoh, B. C., and Davis Clements, L.: Densities of vegetable oils and fatty acids, J. Am. Oil Chem. Soc., 69, 1184–1188, https://doi.org/10.1007/BF02637677, 1992.

Ovadnevaite, J., Zuend, A., Laaksonen, A., Sanchez, K. J., Roberts, G., Ceburnis, D., Decesari, S., Rinaldi, M., Hodas, N., Facchini, M. C., Seinfeld, J. H., and O'Dowd, C.: Surface tension prevails over solute effect in organic-influenced cloud droplet activation, Nature, 546, 637–641, https://doi.org/10.1038/nature22806, 2017.

Pitzer, K. S., Peiper, J. C., and Busey, R. H.: Thermodynamic Properties of Aqueous Sodium Chloride Solutions, J. Phys. Chem. Ref. Data, 13, 1–102, https://doi.org/10.1063/1.555709, 1984.

Prisle, N. L., Raatikainen, T., Sorjamaa, R., Svenningsson, B., Laaksonen, A., and Bilde, M.: Surfactant partitioning in cloud droplet activation: a study of C8, C10, C12 and C14 normal fatty acid sodium salts, Tellus B, 60, 416–431, https://doi.org/10.1111/j.1600-0889.2008.00352.x, 2008.

Prisle, N. L., Raatikainen, T., Laaksonen, A., and Bilde, M.: Surfactants in cloud droplet activation: mixed organic-inorganic particles, Atmos. Chem. Phys., 10, 5663–5683, https://doi.org/10.5194/acp-10-5663-2010, 2010.

Prisle, N. L., Dal Maso, M., and Kokkola, H.: A simple representation of surface active organic aerosol in cloud droplet formation, Atmos. Chem. Phys., 11, 4073–4083, https://doi.org/10.5194/acp-11-4073-2011, 2011.

Pátek, J., Hrubý, J., Klomfar, J., Součková, M., and Harvey, A. H.: Reference Correlations for Thermophysical Properties of Liquid Water at 0.1 MPa, J. Phys. Chem. Ref. Data, 38, 21–29, https://doi.org/10.1063/1.3043575, 2009.

Rogers, P. S. Z. and Pitzer, K. S.: Volumetric Properties of Aqueous Sodium Chloride Solutions, J. Phys. Chem. Ref. Data, 11, 15–81, https://doi.org/10.1063/1.555660, 1982.

Rohatgi, A.: Webplotdigitizer: Version 4.5, https://automeris.io/WebPlotDigitizer, accessed: 2021-10-1 – 2021-10-12, 2021.

Szyszkowski, B.: Experimentelle Studien über kapillare Eigenschaften der wässerigen Lösungen von Fettsäuren., Zeitschrift für Physikalische Chemie, 64U, 385–414, https://doi.org/doi:10.1515/zpch-1908-6425, 1908.

Vanhanen, J., Hyvärinen, A.-P., Anttila, T., Raatikainen, T., Viisanen, Y., and Lihavainen, H.: Ternary solution of sodium chloride, succinic acid and water; surface tension and its influence on cloud droplet activation, Atmos. Chem. Phys., 8, 4595–4604, https://doi.org/10.5194/acp-8-4595-2008, 2008.

Vepsäläinen, S., Calderón, S. M., Malila, J., and Prisle, N. L.: Comparison of six approaches to predicting droplet activation of surface active aerosol – Part 1: moderately surface active organics, Atmos. Chem. Phys., 22, 2669–2687, https://doi.org/10.5194/acp-22-2669-2022, 2022.

Vikingstad, E., Skauge, A., and Høiland, H.: Partial molal volumes and compressibilities of the homologous series of sodium alkylcarboxylates, R6COONa–R13COONa, in aqueous solution, J. Colloid Interface Sci., 66, 240–246, https://doi.org/10.1016/0021-9797(78)90301-6, 1978.

Wen, X., Lauterbach, J., and Franses, E. I.: Surface Densities of Adsorbed Layers of Aqueous Sodium Myristate Inferred from Surface Tension and Infrared Reflection Absorption Spectroscopy, Langmuir, 16, 6987–6994, https://doi.org/10.1021/la991326s, 2000.

Young, T. F. and Smith, M. B.: Thermodynamic Properties of Mixtures of Electrolytes in Aqueous Solutions, J. Phys. Chem., 58, 716–724, https://doi.org/10.1021/j150519a009, 1954.

Zhang, C., Tian, J., Zheng, M., Yi, H., Zhang, L., and Liu, S.: A new corresponding state-based correlation for the surface tension of organic fatty acids, Mod. Phys. Lett. B, 32, 1750 361, https://doi.org/10.1142/S0217984917503614, 2018.